# analytical chemistry

Article

pubs.acs.org/ac

Direct Measurement of the In-Plane Thermal Diffusivity of Semitransparent Thin Films by Lock-In Thermography: An Extension of the Slopes Method

Alexandra Philipp, Nelson W. Pech-May,*[ORCID] Bernd A. F. Kopera, Anna M. Lechner, Sabine Rosenfeldt, and Markus Retsch*[ORCID]

Department of Chemistry, University of Bayreuth, Universitaetsstrasse 30, 95447 Bayreuth, Germany

S *Supporting Information*

ABSTRACT: We present an extension of the well-known slopes method for characterization of the in-plane thermal diffusivity of semitransparent polymer films. We introduce a theoretical model which considers heat losses due to convection and radiation mechanisms, as well as semitransparency of the material to the exciting laser heat source (visible range) and multiple reflections at the film surfaces. Most importantly, a potential semitransparency of the material in the IR detection range is also considered. We prove by numerical simulations and by an asymptotic expansion of the surface temperature that the slopes method is also valid for any semitransparent film in the thermally thin regime. Measurements of the in-plane thermal diffusivity performed on semitransparent polymer films covering a wide range of absorption coefficients (to the exciting wavelength and in the IR detection range of our IR camera) validate our theoretical findings.
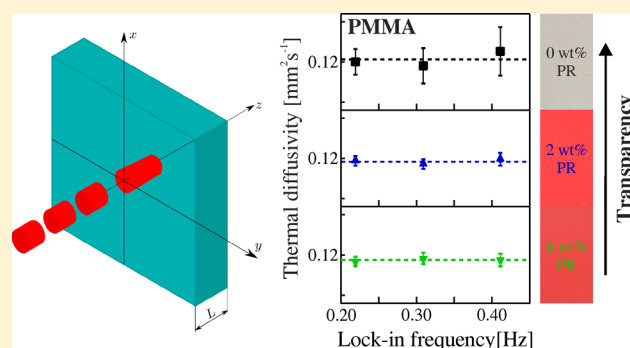
Lock-in thermography is a well-known technique for accurate determination of the in-plane thermal diffusivity of solids.[1−4] In recent decades, it has attracted the attention of scientists due to its noncontact and noninvasive attributes. Moreover, lock-in thermography has shown versatility for materials characterization, in nondestructive testing and evaluation as well as in biomedical applications.[5,6] In particular, for thermal characterization of isotropic solids, the "slopes method"[2,7] has been widely used. Therefore, a freestanding sample is periodically heated by a focused optical source. The temperature oscillations as a function of the radial coordinate are detected, typically using an infrared (IR) camera. The thermographic signal (amplitude T and phase Ψ) is either derived from the front-face[2] or the rear-face configuration,[1] i.e., from the nonilluminated face. The thermographic signals (ln(amplitude) and phase) far from the heating spot vary linearly with radial distance under the precondition of isotropic opaque thin films in the thermally thin regime (film thickness ≪ thermal diffusion length). Moreover, the product between the amplitude slope and the phase slope is independent of convective and radiative heat losses. Consequently, it can be used for the determination of the thermal diffusivity of a film if heat conduction to the gas is negligible.[1,8] Thus, the slopes method is well-suited for measurement of the in-plane thermal diffusivity of high thermal conductors,[4,9−11] whereas it overestimates the in-plane thermal diffusivity of low thermal conductors.[1] This overestimate is produced by the large conductive heat losses from the low conductor surface to the surrounding gas. However, the overestimation can be avoided by measuring the sample under vacuum conditions.

Even though the characterization of opaque samples using lock-in thermography has been widely explored, there is almost no attempt in the literature considering the study of semitransparent samples without a coating.[2] Instead, for measuring the in-plane thermal diffusivity of semitransparent films, it is recommended to coat the sample with a thin opaque layer to be able to use the opaque lock-in models. However, there are some cases in which coating the semitransparent material is not an option. For these applications, such as in situ monitoring of the thermal properties evolution of a polymer film or fiber under stretching, a complete model is required which takes into account the effects of the film semitransparency (to the excitation wavelength and in the infrared range of the IR detector or camera) on the thermographic signal.

In this work, we extend the use of lock-in thermography to the measurement of the in-plane thermal diffusivity of semitransparent thin films of isotropic low thermally conductive materials (such as polymers) without coating. A 2D heat conduction model is considered, which includes heat losses to the surrounding atmosphere, semitransparency of the sample to the exciting wavelength, multiple reflections at the sample

surfaces, as well as the effect of its semitransparency through the IR window of the IR camera used.

In addition to our theoretical work, we performed thermal diffusivity measurements with a home-built lock-in thermography setup. We used three different polymers covering a wide range of absorption properties: poly(methyl methacrylate) (PMMA), low-density polyethylene (LDPE), and polyether ether ketone (PEEK). We chose PMMA as the material because of its low absorption of visible light and high absorption of IR radiation. Thin LDPE films show semitransparency in both the visible and relevant IR wavelength range. We tuned the optical properties of these two materials with the addition of a red dye. The purchased PEEK films are also low absorbers of the visible light. Since their absorption of IR radiation depends on the sample thickness, we measured PEEK films with four different thicknesses.

◼ MODELING AND EXPERIMENTAL SECTION

Modeling. *Heat Conduction through a Semitransparent Film.* Consider a semitransparent film of thickness L, heated by a focused Gaussian laser of wavelength λ and power P_0 modulated at frequency f. The focused beam has the radius a (measured at $1/e^2$). In addition, this film is thermally isotropic and is in a vacuum. Under this circumstance, heat conduction to the surrounding air can be neglected in the model. Figure 1 shows the described situation.
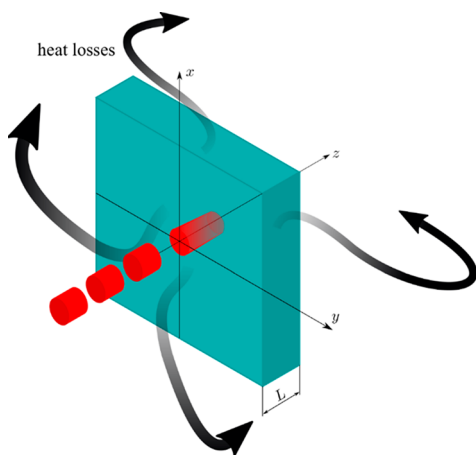
Figure 1. Semitransparent film heated by a focused, modulated Gaussian laser beam. The black arrows indicate heat losses to the environment.

The surface temperature at $z = 0$ (front-face temperature) can be expressed as (a detailed derivation is provided in the Supporting Information)

$$S(r, 0, \omega) = F\frac{P_0}{2\pi K}\frac{(1 - R)\alpha\gamma}{1 - R^2 e^{-2\alpha L}} \int_0^\infty \delta J_0(\delta r)\frac{e^{-(\delta a)^2/8}}{(\beta^2 - \alpha^2)E_0}$$
$$\times \left\{-\frac{A_0}{\beta - \gamma}(1 - e^{(\beta-\gamma)L}) + \frac{B_0}{\beta + \gamma}(1 - e^{-(\beta+\gamma)L})\right.$$
$$+ \frac{E_0}{\alpha + \gamma}(1 - e^{-(\alpha+\gamma)L}) - Re^{-2\alpha L}\left[-\frac{A_1}{\beta - \gamma}(1 - e^{(\beta-\gamma)L})\right.$$
$$\left.\left. + \frac{B_1}{\beta + \gamma}(1 - e^{-(\beta+\gamma)L}) - \frac{E_0}{\alpha - \gamma}(1 - e^{(\alpha-\gamma)L})\right]\right\}d\delta \quad (1)$$

where $\omega = 2\pi f$, r is the radial coordinate, and K is the thermal conductivity of the film. F includes the effect of the IR emissivity, sensor area, IR detection range, and the derivative of the Planck distribution at room temperature. R is the reflectance, and α is the absorption coefficient of the film, both taken at the laser wavelength. γ is an effective IR absorption coefficient, which averages the IR absorption over the detection range of our IR camera. δ is the Hankel space variable; $J_0(\cdot)$ is the Bessel function of zero order, and $\beta^2 = \delta^2 + \frac{i\omega}{D}$. D is the thermal diffusivity of the film. All coefficients A_0, A_1, B_0, B_1, and E_0 are computed explicitly in the Supporting Information, in terms of the thermal diffusivity, modulation frequency, heat convective−radiative losses, and optical absorption.

The surface temperature at $z = L$ (rear-face temperature) reads

$$S(r, L, \omega) = F\frac{P_0}{2\pi K}\frac{(1 - R)\alpha\gamma e^{-\gamma L}}{1 - R^2 e^{-2\alpha L}} \int_0^\infty \delta J_0(\delta r)\frac{e^{-(\delta a)^2/8}}{(\beta^2 - \alpha^2)E_0}$$
$$\times \left\{-\frac{A_0}{\beta + \gamma}(1 - e^{(\beta+\gamma)L}) + \frac{B_0}{\beta - \gamma}(1 - e^{-(\beta-\gamma)L})\right.$$
$$+ \frac{E_0}{\alpha - \gamma}(1 - e^{(\gamma-\alpha)L}) - Re^{-2\alpha L}\left[-\frac{A_1}{\beta + \gamma}(1 - e^{(\beta+\gamma)L})\right.$$
$$\left.\left. + \frac{B_1}{\beta - \gamma}(1 - e^{-(\beta-\gamma)L}) - \frac{E_0}{\alpha + \gamma}(1 - e^{(\alpha+\gamma)L})\right]\right\}d\delta \quad (2)$$

The integrals in eqs 1 and 2 cannot be solved in a closed form, not even in the thermally thin regime ($\mu \gg L$), i.e., when the thermal diffusion length ($\mu = \sqrt{D/(\pi f)}$) is much larger than the actual thickness of the film (L). Thus, it is hard to prove the validity of the slopes method for semitransparent films. Up to now, it has been confirmed for the optically opaque case.[1]

However, it is reliable to do numerical simulations to show the validity of the slopes method for semitransparent films in the thermally thin regime. In this work, we perform simulations for the rear-face configuration, which corresponds to our experimental setup. Moreover, in the thermally thin regime, we have shown the numerical equivalence between the front-face and rear-face temperatures (see Figure S1 of the Supporting Information).

Mendioroz et al.[1] showed that the radial temperature profile for an optically opaque film in the thermally thin regime far from the punctual heating spot ($a = 0$) can be written as

$$T(r \to \infty, 0, \omega) \approx \sqrt{\frac{\pi}{2}}\frac{e^{-\sigma r}}{\sqrt{\sigma r}} \quad (3)$$

where $\sigma^2 = \frac{2h}{KL} + \frac{i\omega}{D}$ and h is the combined coefficient due to convection and radiation losses. From eq 3, it can be shown that the slopes method (product of the amplitude and phase slopes) gives the thermal diffusivity of the film, overcoming the effect of the heat losses. In general, for a given complex number $\sigma^2 = u + \frac{i\omega}{D}$, such that $u \in \mathbb{R}$, ω and D are positive real numbers. It is straightforward to show that the product of its real part $\Re\{\sigma\}$ and its imaginary part $\Im\{\sigma\}$ is independent of u, i.e., $\Re\{\sigma\}\cdot\Im\{\sigma\} = \frac{\omega}{2D}$.

On the other hand, the asymptotic behavior of the Hankel integrals involved in eqs 1 and 2 can be explored.[12,13] Consider a Hankel integral of zero order

$$I_0(b) = \int_0^\infty \phi(x)J_0(bx)\mathrm{d}x \quad b \to \infty \tag{4a}$$

This is an asymptotic expansion that when $b \to \infty$ can be expressed as[12]

$$I_0(b \to \infty)$$
$$= \frac{1}{b}\sum_{s=0}^\infty \frac{(-1)^{1+s}\phi^{(s)}(0)}{s!} \frac{\Gamma\left[\left(\frac{1}{2}\right)(1+s)\right]}{\Gamma\left[\left(\frac{1}{2}\right)(1-s)\right]}\left(\frac{2}{b}\right)^s + \Delta_0(b) \tag{4b}$$

where the first term (infinite summation) is the Poincaré asymptotic expansion (PAE) of the integral in eq 4a and is a series expansion containing integer powers of $1/b$. $\phi^s(0)$ represents the sth derivative of $\phi(x)$ evaluated at $x = 0$, and $\Gamma(\cdot)$ is the gamma function. The second term takes into account the exponentially small decaying terms of the integral. For odd functions $\phi(-x) = -\phi(x)$, the PAE equals zero, and only the exponentially small terms are relevant for the asymptotic expansion. The $\Delta_0(b)$ term can be obtained using the McClure−Wong distributional method.[13] For meromorphic functions, as is our case, it reads

$$\Delta_0(b) = \mathrm{i}\pi \sum_{j=0}^m \mathrm{Res}\{H_0^{(1)}(bz)\phi(z^2)z;\ z = a_j\} \tag{5}$$

where $H_0^{(1)}(\cdot)$ is the Hankel function of first class and zero order. $\mathrm{Res}\{f(z);\ z = a_j\}$ stands for the residues of $f(z)$ evaluated at $z = a_j$, and a_j is the jth pole of $\phi(z^2)$ located in the upper half of the complex plane.

Consider a semitransparent film, in the thermally thin regime, illuminated by a punctual laser source ($a = 0$). The asymptotic expansion of the front-face thermographic signal $S(r \to \infty, 0, \omega)$ can be obtained by computation of the residues appearing the integral in eq 1. The terms which contain poles in eq 1 are linear combinations of

$$S(r \to \infty, 0;\ \omega) \sim$$
$$\int_0^\infty \frac{\delta J_0(\delta r)}{\left(\delta^2 - \alpha^2 + \mathrm{i}\frac{\omega}{D}\right)\left(\delta^2 - \gamma^2 + \mathrm{i}\frac{\omega}{D}\right)\left(\delta^2 + \frac{2h}{KL} + \mathrm{i}\frac{\omega}{D}\right)}\mathrm{d}\delta \tag{6}$$

Following eq 5 we obtain

$$S(r \to \infty, 0;\ \omega) \sim \frac{e^{-\sigma_\alpha r}}{\sqrt{\sigma_\alpha r}} + \frac{e^{-\sigma_\gamma r}}{\sqrt{\sigma_\gamma r}} + \frac{e^{-\sigma_h r}}{\sqrt{\sigma_h r}} \tag{7}$$

where $\sigma_\alpha^2 = -\alpha^2 + \frac{i\omega}{D}$, $\sigma_\gamma^2 = -\gamma^2 + \frac{i\omega}{D}$ and $\sigma_h^2 = \frac{2h}{KL} + \frac{i\omega}{D}$. Note that if the three real parts are of the same order of magnitude, then the expression in eq 7 reduces to a single exponential decaying term

$$S(r \to \infty, 0;\ \omega) \sim \frac{e^{-\sigma r}}{\sqrt{\sigma r}} \tag{8}$$

where $\sigma^2 = u + \frac{i\omega}{D}$ and u is a combination of α, γ, and $2h/(KL)$. This means that the slopes method holds for this particular case. On the other hand, if any of the real parts are larger than the others, the corresponding term in eq 7 can be dropped, because its amplitude is exponentially small with respect to the others. Accordingly, eq 7 always can be reduced to eq 8 for a suitable value of u. As mentioned before, the value of u does not influence

the product of the real and imaginary parts of σ. Thus, we have shown that the slopes method $m_{\ln(|T_\sqrt{r}|)} \cdot m_\Psi = \frac{\pi f}{D}$ is also applicable for semitransparent films in the thermally thin regime, using a punctual excitation source.

Experimental Section. *Materials.* Poly(methyl methacrylate) Plexiglas 7N (PMMA; Evonik), low-density polyethylene Purell PE 1840H (LDPE; LyondellBasell), tetrahydrofuran (THF; >99.9%; Sigma-Aldrich), and phenol red (PR; Alfa Aesar) were used as received. Amorphous polyether ether ketone (PEEK) films with a thickness of 25, 50, 75, and 250 μm were purchased from www.goodfellow.com; potassium bromide (KBr) round cell windows were ordered from Sigma-Aldrich.

Preparation of Thin, Freestanding Films for Lock-In Thermography. Freestanding PMMA films were prepared from solution. Therefore, 30 wt % PMMA was dissolved in THF under magnetic stirring. To obtain red PMMA films 2 and 6 wt % PR (with regard to the amount of PMMA), respectively, were added to PMMA before dissolution in THF. Then, the PMMA solution was cast on a glass substrate using the doctor-blade method. After drying for 48 h, the film was removed from the glass substrate and cut into pieces of appropriate sizes. The thickness of the PMMA films was around 200 μm. The fabrication of the freestanding LDPE films is composed of the following steps: compounding, injection molding, and hot pressing. First, LDPE pellets and PR powder were mixed under N_2 flow in a twin-screw compounder with a stirring speed of 40 rpm and at a temperature of 200 °C. Second, the compounded material was directly filled into the injection unit. Discs with a diameter of ∼27 mm and a thickness of ∼1 mm were fabricated using an injection force of 6 kN and a tool temperature of 20 °C. Finally, thin, freestanding LDPE films were obtained by hot pressing of the discs at a temperature of 200 °C and subsequent cooling to room temperature. In this way, LDPE films with 0, 2, and 6 wt % PR, respectively, were prepared. The thickness of the LDPE films was around 200 μm. Photographs of the PMMA and LDPE thin films with various contents of PR are depicted in Figures S3 and S4. PEEK films were cleaned and cut into pieces.

Characterization Methods. In-plane thermal diffusivity measurements on thin, freestanding films ($\sim$ 200 μm) were conducted using a home-built lock-in thermography (LIT) setup (Figure S4). The sample was heated by a laser beam (Genesis MX 488-1000 SLM OPS, Coherent, λ = 488.1 nm) focused onto the sample surface by a lens of 150 mm focal length. The amplitude of the laser was modulated in sine waveform using a Rigol waveform generator DG1022A. The emitted infrared (IR) radiation of the sample surface is detected by an Infratec VarioCAM HD research IR camera (7.5−14 μm). The camera is equipped with a close-up lens. In this configuration, the minimum spatial resolution is 29 μm at a working distance of 33 mm. To avoid heat losses due to conduction and convection into the environment, all samples were measured under vacuum conditions ($\sim$3 × 10^{-3} mbar). However, heat losses due to radiation still remain. LIT measurements were performed using Infratec's IRBISactiveon-line software. Transparent samples (PMMA and LDPE without phenol red as well as all PEEK films) were coated with a 20 nm carbon layer for enhanced laser absorption. The coating of the sample was facing the infrared camera. The influence of the carbon coating on the absorption of light in the IR and UV−vis range is shown in Figure S6. In the case of the fabricated polymeric films (PMMA and LDPE), we measured three
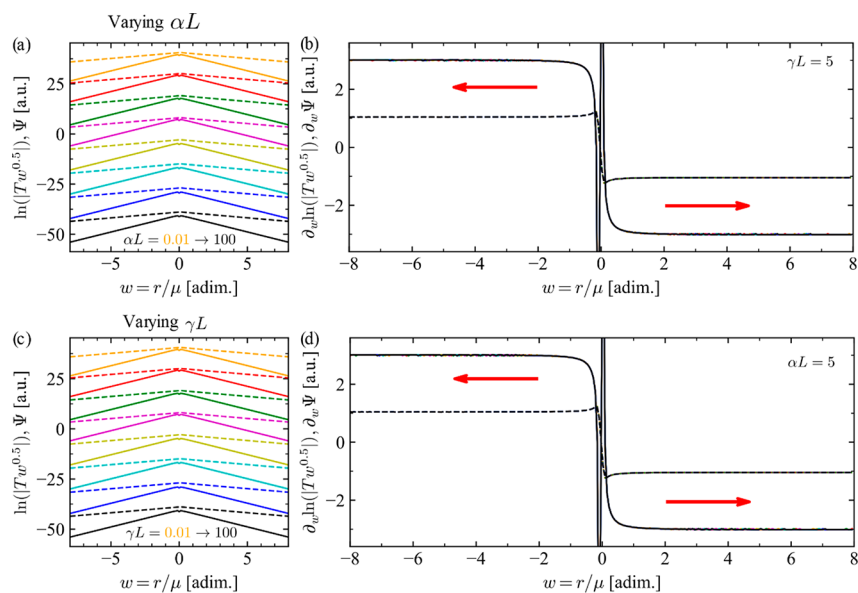
Figure 2. (a) Plots of $\ln(|T\sqrt{w}|)$ (continuous lines) and Ψ (dashed lines) as a function of the normalized radial profile $w = r/\mu$. A wide range of absorption coefficients is explored at a fixed IR absorption: $\gamma L = 5$. (b) Derivatives of amplitudes (continuous lines) and phases (dashed lines) with respect to w, for different absorption coefficients, are explored. Note that results overlap. (c) Plots of $\ln(|T\sqrt{w}|)$ (continuous lines) and Ψ (dashed lines) as a function of the normalized radial profile $w = r/\mu$. A wide range of IR absorption coefficients is explored at a fixed optical absorption: $\alpha L = 5$. (d) Derivatives of amplitudes (continuous lines) and phases (dashed lines) with respect to w, for the different IR absorption coefficients, are explored. Note that the results overlap.

different films per sample; in the case of the purchased PEEK films, we measured only one film per sample.

UV−vis measurements were conducted on an Agilent Cary 5000 spectrometer in the transmission mode. Absorption spectra were recorded from 380 to 800 nm. The data interval was fixed to 1 nm, with averaging for 100 ms. Each measured sample was normalized with a suitable reference (control): For the freestanding polymers, the direct lamp spectrum in air was used. For the measurement of the carbon coating, an uncoated KBr disc was used. The phenol red powder was measured by applying a thin layer on transparent adhesive tape with the same tape as reference. The same polymeric samples as characterized by lock-in thermography were investigated.

A Bruker Vertex 70 FT-IR spectrometer was used for absorption spectra acquisition. The polymeric samples, as well as a carbon-coated KBr window, were measured in transmission mode. To get the IR absorbance of the pure carbon layer, an uncoated KBr window with the same thickness as the uncoated one was used as a reference. Furthermore, an ATR-IR spectrum of phenol red powder was recorded. All samples were measured in the wavenumber range of the spectral range of the infrared camera (data interval, 4 cm^{-1}; averaging, 32 measurements).

■ RESULTS AND DISCUSSION

Numerical Simulations. Here we present numerical simulations of the radial temperature profiles based on eq 2. A thin polymeric film ($K = 0.15$ W m^{-1} K^{-1}, $D = 0.10$ mm^2 s^{-1}) with thickness $L = 25\ \mu$m is considered. The laser power is set to $P_0 = 50$ mW at a modulation frequency $f = 0.10$ Hz. This gives a thermal diffusion length $\mu = 564\ \mu$m; i.e., the film is in the thermally thin regime ($\mu \gg L$). A typical value is used for the combined heat transfer coefficient $h = 15$ W m^{-2} K^{-1}.[8,14]

Figure 2a shows simulations of a surface temperature radial profile for a semitransparent film, considering a fixed IR absorption coefficient such that $\gamma L = 5$. The absorption

coefficient to the incident laser wavelength is varied over a wide range: $0.01 \leq \alpha L \leq 100$. The laser beam is focused on the film surface with a radius $a = 0.1\mu$. The temperature profiles for the "amplitude" $\ln(|T\sqrt{w}|)$ and phase Ψ are presented with a vertical shift and in ascending order of αL from top to bottom.

The derivatives of the "amplitude" $\partial_w \ln(|T\sqrt{w}|)$ and phase $\partial_w \Psi$ with respect to the normalized radial profile are antisymmetric around the beam spot position ($r = 0$), as depicted in Figure 2b. Both derivatives reach a constant value above $r = 2\mu$ (and below $r = -2\mu$), as indicated by the red arrows. Thus, $|r| \geq 2\mu$ corresponds to the linear part of the temperature profiles shown in Figure 2a. Two red arrows mark these intervals. Within the region $0 \leq r \leq 2\mu$, the amplitude derivative shows a concave upward behavior and is discontinuous at $r = 0$. This discontinuity is due to the logarithmic function. In contrast, the phase derivative is concave downward away from the beam spot; it shows an abrupt change to concave upward near $r = 0$ and is continuous at the beam spot position. Moreover, the values of the derivatives for the different absorption coefficients to the exciting wavelength are equal, as they are all superimposed in Figure 2b. This means that the difference between the slopes of the amplitude $\ln(|T\sqrt{w}|)$ and phase Ψ profiles (for $|r| \geq 2\mu$) is due to the heat losses independent of αL.

Simulations presented in Figure 2c are similar to those in Figure 2a, but in this case, the optical absorption coefficient to the exciting wavelength is fixed ($\alpha L = 5$), and a wide range of IR absorption coefficients are explored: $0.01 \leq \gamma L \leq 100$. The same radius $a = 0.1\mu$ is used for the focused beam. The simulations are vertically shifted in ascending order of γL from top to bottom.

The corresponding "amplitude" and phase derivatives are shown in Figure 2d. The same characteristics as described in Figure 2b are found. In this case, the values of the derivatives for the different IR absorption coefficients are equal, as they are all superimposed. This means that the difference between the
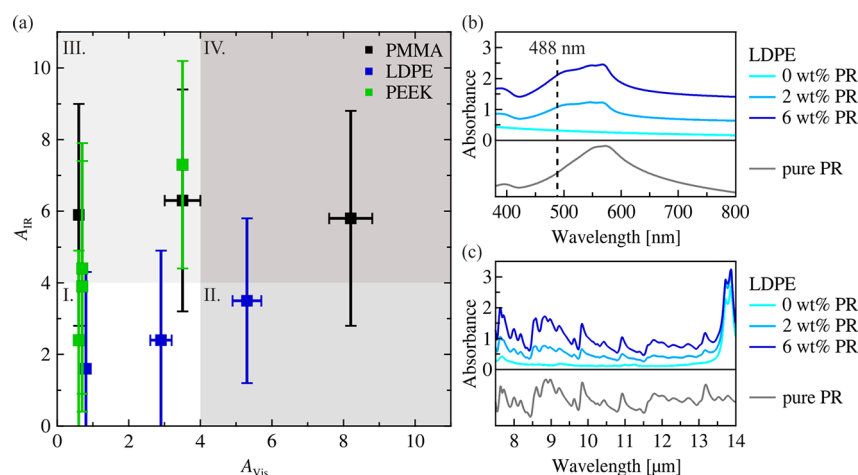
Figure 3. (a) Plot of A_{IR} versus A_{Vis} of all polymeric thin films. The error bars of A_{IR} arise from measuring three films per sample (except for PEEK) and from averaging over the spectral wavelength range of the infrared camera (7.5−14 μm); the error bars of A_{Vis} arise from measuring three films per sample (except for PEEK). Area I marks the (semi)transparent A_{Vis} and A_{IR} range, and area II marks the opaque A_{Vis} range and (semi)transparent A_{IR} range. Area III marks the (semi)transparent A_{Vis} range and opaque A_{IR} range, and area IV marks the opaque A_{Vis} and A_{IR} range. Exemplary (b) IR and (c) UV−vis absorbance spectra of LDPE with 0, 2, and 6 wt % phenol red (PR) as well as the spectra of pure PR powder are shown. The dashed line at 488 nm marks the wavelength of the incident laser used in lock-in measurements.

Table 1. Summary of A_{Vis} and A_{IR} values of PMMA and LDPE Films with Various PR Contents, and PEEK Samples with Different Film Thicknesses[a]

		A_{Vis}[c]	A_{IR}[d]	exciting laser light	IR radiation
PMMA	0 wt % PR[b]	0.6 ± 0.1	>3.5[e]	semitransparent	opaque
	2 wt % PR	3.5 ± 0.5	>3.5[e]	semitransparent	opaque
	6 wt % PR	8.2 ± 0.6	>3.5[e]	opaque	opaque
LDPE	0 wt % PR[b]	0.8 ± 0.1	1.6 ± 2.7	semitransparent	semitransparent
	2 wt % PR	2.9 ± 0.3	2.4 ± 2.5	semitransparent	semitransparent
	6 wt % PR	5.3 ± 0.4	3.5 ± 2.3	opaque	semitransparent
PEEK	25 μm film[b]	0.6	2.4 ± 2.5	semitransparent	semitransparent
	50 μm film[b]	0.7	>3.5[e]	semitransparent	opaque
	75 μm film[b]	0.7	>3.5[e]	semitransparent	opaque
	250 μm film[b]	3.5	>3.5[e]	semitransparent	opaque

[a]Classification of the optical properties regarding the exciting laser light and IR radiation in "semitransparent" or "opaque". [b]With 20 nm carbon coating. [c]Value at 488 nm. [d]Average value for 7.5−14 μm; error is the standard deviation of the average value. [e]Above the detection limit. In the case of the PMMA and LDPE samples, three films were measured, and an average value of A_{Vis} and A_{IR} was calculated.

slopes of the amplitude $\ln(|T\sqrt{w}|)$ and phase Ψ profiles is also due to the heat losses, independent of γL. To validate the above results, further simulations for a wide range of both absorption coefficients were performed (see Supporting Information).

We have found that the product between the amplitude derivative $\partial_w \ln(|T\sqrt{w}|)$ and phase derivative $\partial_w \Psi$, for $|r| \geq \mu$, is constant and independent of the optical absorption to the exciting wavelength and to the optical absorption in the IR detection range; i.e., this result is also correct in the optically opaque limit. Consequently, on the basis of the slopes method for optically opaque films in the thermally thin regime,[1] we conclude that, for any semitransparent or opaque film in the thermally thin regime and far from the excitation beam spot, $|r| \geq \mu$:

$$\partial_r \ln(|T\sqrt{r}|) \cdot \partial_r \Psi = m_{\ln(|T\sqrt{r}|)} \cdot m_\Psi = \frac{\pi f}{D} \quad (9)$$

This confirms our theoretical expectation as outlined above.

Lock-In Thermography Measurements. To validate our theoretical results experimentally, we measured three different polymers covering a wide range of IR absorption coefficients and optical absorption coefficients to the exciting wavelength:

poly(methyl methacrylate) (PMMA), low-density polyethylene (LDPE), and polyether ether ketone (PEEK). To tune the optical properties of PMMA and LDPE, we added 2 and 6 wt % phenol red (PR), respectively (Figure S3). Furthermore, PEEK films with different thicknesses, i.e., 25, 50, 75, and 250 μm, were investigated.

In Figure 3a, a plot of the IR absorption $(A_{IR} = \gamma L/\ln(10))$ as a function of the optical absorption $(A_{Vis} = \alpha L/\ln(10))$ to the exciting wavelength of all samples is shown. In Table 1, the corresponding values are listed. Furthermore, the samples are classified in "semitransparent" or "opaque" regarding their optical properties to the exciting laser light and IR radiation.

Figure 3a is divided into four areas dependent on the optical properties of the material:

(I) (semi)transparent to both IR radiation in the wavelength range of the IR camera (7.5−14 μm) and the exciting wavelength of the laser (488 nm),

(II) (semi)transparent to the IR radiation and opaque to the exciting wavelength,

(III) opaque to the IR radiation and (semi)transparent to the exciting wavelength, and

(IV) opaque to both IR radiation and exciting wavelength.
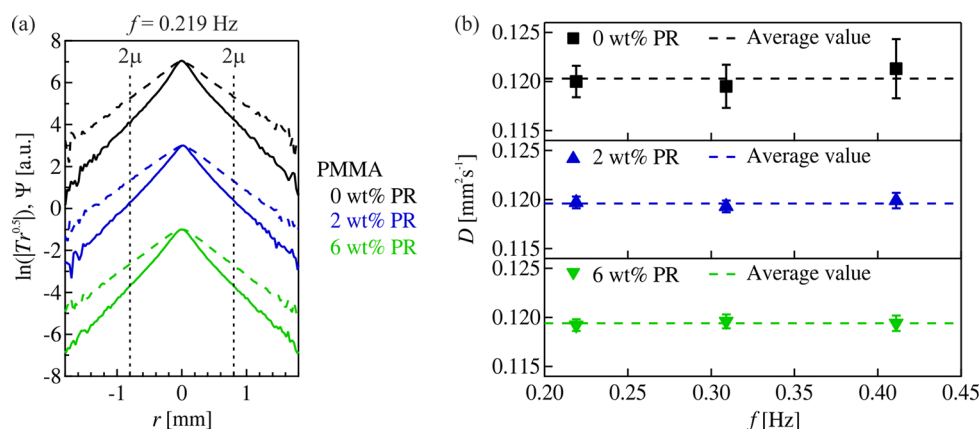
Figure 4. Exemplary measurement data of a PMMA film with 0, 2, and 6 wt % phenol red (PR), respectively. (a) Plots of $\ln(|T\sqrt{w}|)$ (continuous lines) and Ψ (dashed lines) as a function of the radial profile r. The vertical dashed lines at 2μ ($\sim$800 μm) represent the lower fitting boundary used for evaluation of the phase and amplitude profiles. (b) Plots of the thermal diffusivity D against the lock-in frequency f. Error bars are the standard error arising from the fitting of the radial profiles. The dashed lines represent the respective average value.
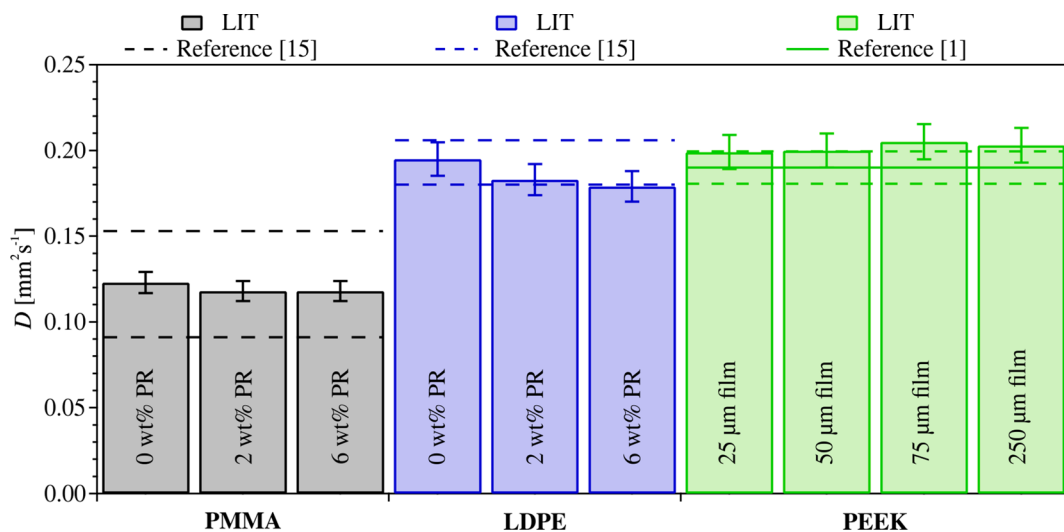
Figure 5. Thermal diffusivity D of PMMA (black bars) and LDPE (blue bars) with 0, 2, and 6 wt % phenol red (PR), respectively. Error bars are 5% uncertainty. The dashed lines represent the lower and upper limits of the reference values for unmodified PMMA and LDPE.[15] The thermal diffusivities of PEEK films with a thickness of 25, 50, 75, and 250 μm are plotted as green bars. Error bars are 5% uncertainty. The corresponding solid line represents the literature value also measured with lock-in thermography. The dashed lines are the 5% uncertainty range given by Mendioroz et al.[1]

As can be seen from this plot, PMMA is opaque to IR radiation and semitransparent (III) or opaque (IV) to the exciting laser light depending on the dye concentration. LDPE, on the other hand, is semitransparent to IR radiation and semitransparent (I) or opaque, due to a higher PR content, (II) to the exciting laser light. Here, the addition of PR enhances not only the absorbance of visible light (Figure 3b) but also the absorbance of IR light (Figure 3c). All PEEK films are semitransparent to the exciting laser light, but either semitransparent (I) or opaque (III) to the IR radiation depending on the sample thickness. IR and UV−vis absorbance spectra of all samples are summarized in Figure S7.

Exemplary lock-in thermography (LIT) measurement data of PMMA with various PR contents (0, 2, 6 wt % PR) are depicted in Figure 4a. Here, temperature profiles for the "amplitude" $\ln(|T\sqrt{w}|)$ and phase Ψ are shown for a lock-in frequency f of 0.219 Hz. To be independent of the optical properties of the thin films, we extracted the phase and "amplitude" slopes above a radial distance of 2μ (vertical dashed lines in Figure 4a). Subsequently, we calculated the thermal diffusivity D for each

frequency using the equation $m_{\ln(|T\sqrt{r}|)} \cdot m_\Psi = \frac{\pi f}{D}$. Fits were done on radial averaged profiles for each phase and amplitude image. In this way, the whole phase and amplitude distribution are evaluated rather than single lines. Figure 4b shows the individual thermal diffusivities with dependence on the used lock-in frequency. The error bars arise from the fitting of the radial profiles. From this data, an average thermal diffusivity is calculated (dashed line). The data in Figure 4b indicates that the PMMA films have similar thermal diffusivities independent of the PR content. Therefore, the slopes method is valid independent of the optical absorption at the exciting wavelength. However, the standard error of the individual thermal diffusivities is larger for the sample without PR due to the lower signal-to-noise ratio of the radial profiles.

The thermal diffusivities determined by LIT are shown in Figure 5. We measured PMMA and LDPE films with 0, 2, and 6 wt % of PR content. Additionally, four PEEK samples with different thicknesses were measured. For all samples, we obtained rather small standard deviations of the thermal

diffusivity. In Figure 5, we plot an uncertainty of 5% as error bars.[1,15]

From our lock-in measurements, we determined an in-plane thermal diffusivity of ∼0.12 mm² s⁻¹ for PMMA independent of the PR content. Thus, the result does not depend on the optical absorption coefficient to the exciting wavelength that changes from semitransparent to opaque with an increasing amount of red dye (Table 1). Similarly, for LDPE with 0, 2, and 6 wt % PR, we found a thermal diffusivity of ∼0.19 mm²s⁻¹. Here, too, we observe no dependence on the optical absorption coefficient for the exciting laser light (Table 1).

We obtained an average thermal diffusivity value of ∼0.20 mm² s⁻¹ for all PEEK samples independent of the film thickness. Consequently, the result is not affected by the IR absorption coefficients that change from semitransparent to opaque with increasing film thickness (Table 1). The PEEK films also serve as reference material for our LIT setup, since literature values are available that were also measured with thermographic methods.[1,16] The literature value of 0.19 mm² s⁻¹ from Mendioroz et al.[1] is plotted as a solid green line in Figure 5; the dashed green lines represent the 5% uncertainty range of this value. We found a low relative deviation of ∼5% between our average value and the literature value. This good agreement proves that correct thermal diffusivity values are obtained even for samples with low optical absorption coefficients for the exciting wavelength.

We note the fundamental difficulty in quantitatively comparing the thermal conductivity of polymer samples reported from different groups. This is an inherent problem owing to the variability of the sample microstructure, which can be strongly altered on the basis of the fabrication and processing conditions. This is particularly true for semicrystalline samples because not only the polymer chain orientation but also the degree of crystallinity can vary significantly. Furthermore, a quantitative characterization of the exact polymer micro-structure is difficult to achieve and often not reported along the measured thermal conductivity values. In addition to the microstructure, the thermal transport characterization technique may also result in systematically differing thermal conductivity values. Consequently, a broad range of typical thermal conductivities are generally accepted for many polymer materials, which lead to the dashed lines for PMMA and LDPE in Figure 5.[15] We report the influence of both issues (sample microstructure and measurement method) on the thermal conductivity value for our samples to provide a more reasonable classification of the absolute thermal conductivity values that we offer (see Supporting Information for further information). We, therefore, compare LIT to xenon flash analysis (XFA) for polymer samples stemming from various preparation conditions. We found for the amorphous PMMA samples no signs of polymer crystallinity (Figure S8) and a comparable polymer microstructure. This led to a good agreement between LIT and XFA (which measure the cross-plane thermal diffusivity) measurements. For the semicrystalline LDPE samples, we did not observe any influence of the PR dye on the degree of crystallinity (see Supporting Information). Yet, the orientation of the crystalline domains is strongly anisotropic and depends on the processing conditions such as hot-pressing and thermal annealing (Figure S10). The XFA measurement results in lower cross-plane thermal diffusivities compared to LIT, which may be caused by the in-plane orientation of the LDPE crystallites. Thermal annealing further alters the LDPE microstructure, as can be seen for the thick XFA samples, which leads to a concomitant increase in thermal diffusivity. Due to the much lower degree of anisotropy upon hot pressing, the thin samples for LIT are less sensitive to the thermal annealing step and, consequently, do not change significantly.

Considering these uncertainties, it becomes clear that we obtained accurate values of thermal diffusivity for uncoated semitransparent samples using the slopes method. These experimental results validate our theoretical expectations discussed in the Numerical Simulations section. Lock-in thermography is, consequently, a powerful and versatile characterization technique to measure thermal transport in thin, freestanding films and fibers, independent of their optical properties.

■ CONCLUSION

In this paper, we developed a two-dimensional heat conduction model which includes, in addition to heat losses to the surrounding atmosphere, also semitransparency of the sample to the exciting wavelength, multiple reflections at the sample surfaces, and the effect of its semitransparency through the infrared (IR) sensitivity of the IR camera used. On the basis of this model, we conducted numerical simulations to investigate separately the effect of semitransparency on the exciting laser light and on the IR wavelength of the IR camera. We found that the well-known slope method, which does not consider semitransparency, is still valid as long as the phase and amplitude slopes are extracted far from the heating spot center ($\gtrsim 2\mu$). We translate our theoretical findings into the measure-ment of three different polymers, poly(methyl methacrylate) (PMMA), low-density polyethylene (LDPE), and polyether ether ketone (PEEK). The optical properties in the visible and IR wavelength ranges of these polymers were varied by their film thickness (PEEK) or by the addition of a red dye (PMMA and LDPE). We obtained thermal diffusivity values which are in good agreement with literature values and independent of the optical absorption properties of the samples. We could, therefore, show that, in the thermally thin regime, the slopes method holds (far from the heating spot center) independent of semitransparency (to the exciting wavelength and in the IR range of the camera). Consequently, the in-plane thermal diffusivity can be measured accurately.

■ ASSOCIATED CONTENT

ⓢ Supporting Information

The Supporting Information is available free of charge on the ACS Publications website at DOI: 10.1021/acs.anal-chem.9b01583.

> Details of the analytical model for a semitransparent film, photographs of polymer samples, UV−vis and IR spectra of all samples as well as the influence of carbon coating, XRD and SAXS data, and reference thermal diffusivity measurements using XFA (PDF)

■ AUTHOR INFORMATION

Corresponding Authors
*E-mail: markus.retsch@uni-bayreuth.de.
*E-mail: nelson.pech@uni-bayreuth.de.
ORCID ⓘ
Nelson W. Pech-May: 0000-0002-5822-482X
Markus Retsch: 0000-0003-2629-8450

Notes

The authors declare no competing financial interest.

REFERENCES

(1) Mendioroz, A.; Fuente-Dacal, R.; Apinaniz, E.; Salazar, A. *Rev. Sci. Instrum.* **2009**, *80* (7), No. 074904.

(2) Zhang, B.; Imhof, R. E. *Appl. Phys. A: Mater. Sci. Process.* **1996**, *62* (4), 323−334.

(3) Salazar, A.; Mendioroz, A.; Fuente, R.; Celorrio, R. *J. Appl. Phys.* **2010**, *107* (4), No. 043508.

(4) Wolf, A.; Pohl, P.; Brendel, R. *J. Appl. Phys.* **2004**, *96* (11), 6306−6312.

(5) Boué, C.; Cassagne, F.; Massoud, C.; Fournier, D. *Infrared Phys. Technol.* **2007**, *51* (1), 13−20.

(6) Rantala, J.; Wu, D.; Busse, G. *Res. Nondestruc. Eval.* **1996**, *7* (4), 215−228.

(7) Fabbri, L.; Fenici, P. *Rev. Sci. Instrum.* **1995**, *66* (6), 3593−3600.

(8) Salazar, A.; Mendioroz, A.; Fuente, R. *Appl. Phys. Lett.* **2009**, *95* (12), 121905.

(9) Muscio, A.; Bison, P. G.; Marinetti, S.; Grinzato, E. *Int. J. Therm. Sci.* **2004**, *43* (5), 453−463.

(10) Pradère, C.; Goyhénèche, J. M.; Batsale, J. C.; Dilhaire, S.; Pailler, R. *Int. J. Therm. Sci.* **2006**, *45* (5), 443−451.

(11) Oksanen, M.; Scholz, R.; Fabbri, L. *J. Mater. Sci. Lett.* **1997**, *16* (13), 1092−1094.

(12) Galapon, E. A.; Martinez, K. M. *Proc. R. Soc. London, Ser. A* **2014**, *470* (2162), 20130529.

(13) Frenzen, C. L.; Wong, R. *Math. Comput.* **1985**, *45* (172), 537.

(14) Kanstad, S. O.; Nordal, P.-E. *Can. J. Phys.* **1986**, *64* (9), 1155−1164.

(15) Granta Design. *CES Edupack*; Cambridge, UK, 2015.

(16) Pech-May, N. W.; Mendioroz, A.; Salazar, A. *NDT&E Int.* **2016**, *77*, 28−34.